Received: 7 October 2021 | Revised: 16 January 2022 | Accepted: 29 January 2022

DOI: 10.1002/cnm.3577

APPLIED RESEARCH

WILEY

Computational study of a novel catheter for liver radioembolization

Julio Ortega[1,2] | **Raúl Antón**[2,3] | **Juan Carlos Ramos**[2] | **Alejandro Rivas**[2] | **Gorka S. Larraona**[2] | **Bruno Sangro**[3] | **José Ignacio Bilbao**[3,4] | **Jorge Aramburu**[2]

[1]Escuela de Ingeniería Mecánica, Pontificia Universidad Católica de Valparaíso, Quilpué, Chile

[2]Universidad de Navarra, Tecnun - Escuela de Ingeniería, Donostia-San Sebastián, Spain

[3]Instituto de Investigación Sanitaria de Navarra, IdiSNA, Pamplona, Spain

[4]Department of Radiology, Clínica Universidad de Navarra, Pamplona, Spain

Correspondence

Raúl Antón, Universidad de Navarra, Tecnun - Escuela de Ingeniería, Donostia-San Sebastián, Spain.

Email: ranton@tecnun.es

Funding information

ANID Scholarship; Spanish Government, Grant/Award Number: DPI 2015-68985-R; Proyecto VRIEA-PUCV, Grant/Award Number: 039.356/2021

Abstract

Radioembolization (RE) is a medical treatment for primary and secondary liver cancer that involves the transcatheter intraarterial delivery of micron-sized and radiation-emitting microspheres, with the goal of improving microsphere deposition in the tumoral bed while sparing healthy tissue. An increasing number of in vitro and in silico studies on RE in the literature suggest that the particle injection velocity, spatial location of the catheter tip and catheter type are important parameters in particle distribution. The present in silico study assesses the performance of a novel catheter design that promotes particle dispersion near the injection point, with the goal of generating a particle distribution that mimics the flow split to facilitate tumour targeting. The design is based on two factors: the direction and the velocity at which particles are released from the catheter. A series of simulations was performed with the catheter inserted at an idealised hepatic artery tree with physiologically realistic boundary conditions. Two longitudinal microcatheter positions in the first generation of the tree were studied by analysing the performance of the catheter in terms of the outlet-to-outlet particle distribution and split flow matching. The results show that the catheter with the best performance is one with side holes on the catheter wall and a closed frontal tip. This catheter promotes a flow-split-matching particle distribution, which improves as the injection crossflow increases.

KEYWORDS

hemodynamics, liver cancer, microcatheter, particle-fluid dynamics, radioembolization, side-holes catheter

1 | INTRODUCTION

Liver cancer is the fourth most common cause of death from cancer and the sixth most frequently diagnosed cancer worldwide.[1] Currently, locoregional therapies are effective cancer treatments, especially for tumours and metastatic liver malignancies.[2,3] One of these therapies is radioembolization (RE), which involves injecting micron-sized ^{90}Y-labelled microspheres into the hepatic artery via a catheter.[4]

Tumours are primarily irrigated by arterial supply, which encourages particles to be directed to the tumour vasculature. This advantageous condition reduces the risk of radiating nontumoral liver tissue.[5] When the micron-sized particles become trapped in the tumour-irrigating vasculature, they deliver locally high doses of radiation to tumours.[6]

Currently, in silico studies are a viable tool for studying haemodynamics-related topics. Specifically, numerical simulations have been used to analyse RE-related topics.[7,8] These studies have shown that particle injection velocity[9,10] and the spatial orientation of the catheter tip[11,12] may play important roles in the particle distribution. Innovative catheter designs have also been numerically assessed, such as an antireflux catheter with an expandable tip. Xu et al.[13] and Aramburu et al.[14] assessed the performance of the antireflux catheter and showed perturbations in haemodynamics at the catheter tip and the subsequent effect on particle motion. There have also been in vitro studies of the performance of an antireflux catheter. For example, van den Hoven et al.[15] compared particle injection with a standard end-hole microcatheter and an antireflux catheter. The results showed that the antireflux catheter developed a centroluminal position and a chaotic particle injection pattern, resulting in a homogeneous particle distribution in several outlets of a surrogate hepatic model.

The most widely used microcatheter is the standard end-hole microcatheter. Aramburu et al.[11] showed that when using this catheter, the particle distribution is dependent on various parameters, for example, a longitudinal or a radial shift in the catheter tip can result in a completely different particle distribution. Another study by Aramburu et al.[14] found that if an antireflux catheter is inserted at a longitudinal point far enough from a bifurcation, the particle distribution tends to match the flow split. This occurs because particles tend to align with the bloodstream and fill the whole cross-sectional area of the lumen of the artery. Hepatic arterial morphology (i.e., high tortuosity) and injection location (i.e., far from a bifurcation) are parameters that improve lumen filling or particle dispersion.

When planning RE therapy, lumen filling can be very interesting, especially if the tumour burden extends to the whole liver. It is well known that tumour tissue has greater arterial perfusion than normal tissue.[16] As a result, more blood is directed towards the tumours. If the interventional radiologist can direct the particles to areas that demand more blood, then the treatment outcome is expected to be successful. In these cases, regardless of the morphology of the hepatic artery or the proximity of a bifurcation near the injection point, a catheter that promotes lumen filling is critical.

In this study, we present a new catheter tip design that promotes lumen filling, which improves the alignment of particle distribution with flow splitting and thus targets tumours. Lumen filling could be achieved with a novel catheter tip design that takes advantage of a crossflow effect between blood flow and particle path lines inside the artery lumen. Particle haemodynamic simulations in an idealised hepatic artery with physiologically realistic boundary conditions were used to assess different tip designs. The interactions of several design factors and their influence on certain responses were assessed by using Design of Experiments (DoE) techniques.

2 | METHODS

2.1 | Computational domain

A three-dimensional idealised geometry of the hepatic artery was used in this study, as shown in Figure 1. This type of arterial geometry can be used as a generalist approach that allows for the independent analysis of the effect of a variable in the microsphere distribution with respect to others.[17]

This geometrical model, which represents a hepatic artery “type I" according to Hiatt's hepatic artery classification,[18] is built with the following geometric parameters: the daughter–parent branch diameter ratio is 0.8, and the average branch length is 35 mm[19]; the angle between the flow direction in the parent vessel and the flow direction in the daughter vessel is 30°[20,21]; and a typical diameter of the proper hepatic artery (PHA) of 5 mm[22] is used, ending with an outlet diameter of 3 mm. The hepatic artery consists of two levels of bifurcations with four outlets in total (see the outlet nomenclature in Figure 1D). Level I corresponds to the PHA, level II corresponds to the right and left hepatic arteries (RHA and LHA), and level III corresponds to the pre-segmental arteries.

A standard end-hole microcatheter is inserted from the inlet boundary. Two catheter tip positions were defined: 10 and 30 mm from the PHA bifurcation (see Figure 1C). A commercially available 2.7-F end-hole microcatheter with outer and inner diameters of 0.90 and 0.65 mm, respectively, was modelled. The studied catheter tip designs, explained in Section 2.6, have the same inner and outer diameters.

The catheter was slightly curved along the *X-Z* plane to obtain an eccentricity of 0.22 in the local plane (injection section angled at 3.43° to the perpendicular plane, see Figure 1B). The eccentricity *e* was determined as shown in Equation (1):

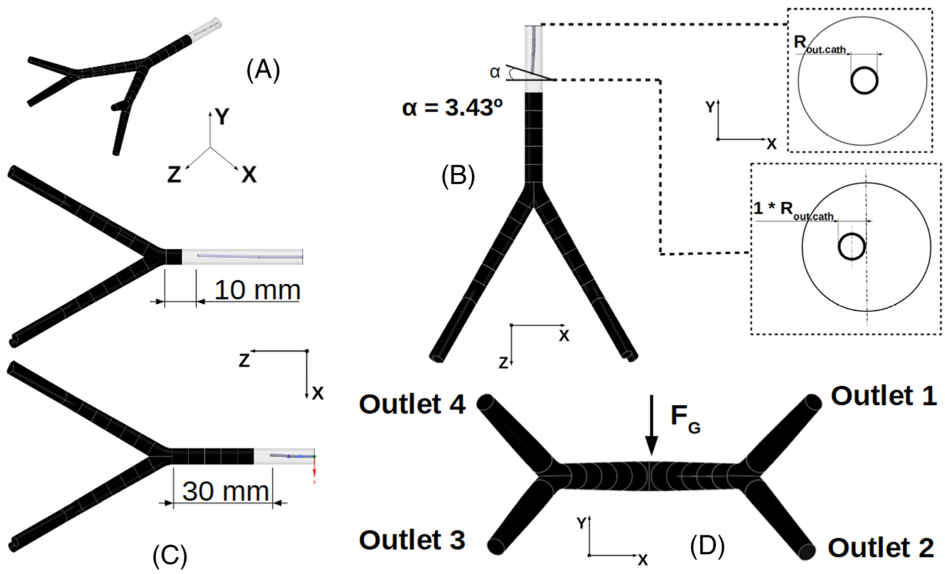

FIGURE 1 Idealised hepatic artery geometry views. (A) Isometric view, (B) top view with the cross-sectional position of the catheter at the inlet and injection section, (C) top view with the two longitudinal positions of the catheter, and (D) front view with outlet nomenclature and gravity vector F_G direction

$$e = \frac{d}{r_{\text{artery}} - r_{\text{outer cath.}}} \tag{1}$$

where d is the radial displacement of the catheter tip (0.45 mm), r_{artery} is the PHA radius (2.5 mm), and $r_{\text{outer cath}}$ is the outer radius of the catheter (0.45 mm).

The geometries were built with the computer-aided design software package SpaceClaim 19.2 (ANSYS® Inc., Canonsburg, PA, USA).

2.2 | Discretization

The 2,858,628-element computational mesh was generated with polyhexahedral elements with a minimum element size of 0.01 mm, a maximum element size of 0.1 mm, and a growth rate of 1.20. A refinement was applied on the walls to capture the boundary layer region.Figure 2 shows a lateral zoom view of the mesh close to the first bifurcation, as well as a cross-sectional view of the mesh in two different cross-sections: in the annular section near the catheter tip and before the PHA bifurcation.

The mesh was created by using the software package ANSYS Fluent Meshing 19.2 (ANSYS® Inc.). A mesh independence analysis was carried out to determine whether the mesh was sufficiently fine. For the analysis, three meshes were used: a coarse mesh, a medium mesh and a fine mesh. The mesh previously described is the medium mesh (2,858,628 elements). The coarse mesh (1,708,392 elements) was generated by multiplying the element size of the medium mesh by $\sqrt[3]{2}$, and the fine mesh (5,594,944 elements) was generated by dividing the element size of the medium mesh by $\sqrt[3]{2}$.

Transient simulations were run using the cancer scenario reported by Aramburu et al.[14] and the simulation characteristics reported in this study, and the area-weighted average wall shear stress (WSS) across the whole arterial wall was computed. With this metric, the differences between the medium and fine meshes with respect to the coarse mesh are 0.0035% and 0.0061%, respectively. The same sensitivity study was used to study the particle distribution in each outlet. Furthermore, in the case of the discrete phase, the average difference between the coarse mesh and the medium mesh is 0.80%, and the average difference between the coarse mesh and the fine mesh is 1.57%. Even though the coarse mesh was good enough for the simulations, the medium mesh was used because the catheter tip designs produce more complex phenomena near the injection point.

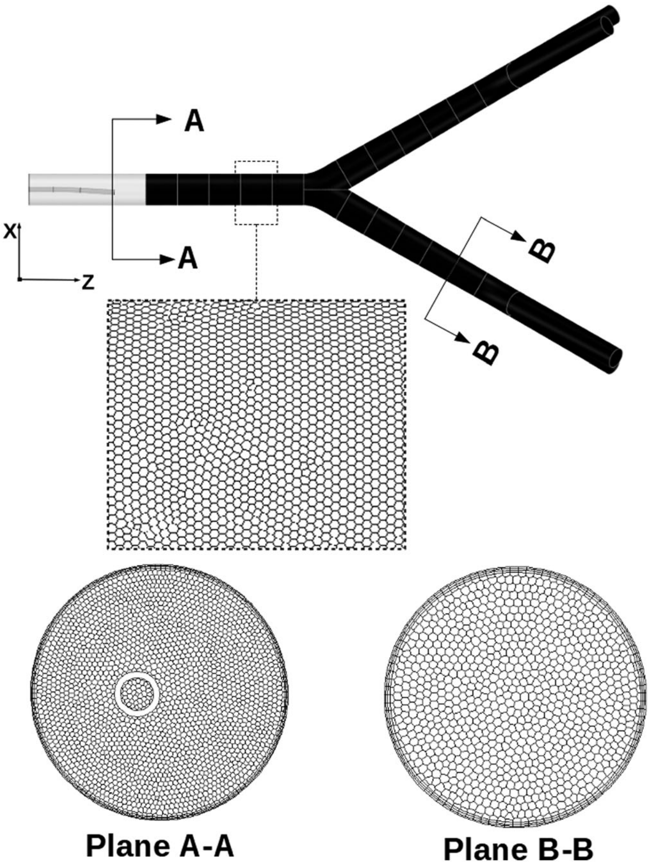

FIGURE 2 Computational mesh around the artery wall at the PHA and details of the mesh in two cross-sections of the computational domain, before and after the bifurcation

2.3 | Governing equations

The governing equations of the haemodynamics were solved for the laminar flow case. Blood was assumed to be an incompressible, non-Newtonian, and isothermal fluid. In this case, the equations of the haemodynamics are the equation of the conservation of mass (Equation (2)) and the equation of the conservation of linear momentum (Equation (3)):

$$\nabla \cdot \mathrm{u} = 0 \tag{2}$$

$$\frac{\partial \mathrm{u}}{\partial \mathrm{t}} + \nabla \cdot (\mathrm{uu}) = \frac{1}{\rho}(-\nabla p + \nabla \cdot \tau) + \mathrm{f} \tag{3}$$

where u is the velocity vector, ρ is the density (1050 kg/m^3), p is the pressure, τ is the stress tensor, and f is the body force vector (per fluid unit mass). The stress tensor, Equation (4), is a function of a shear rate-dependent apparent viscosity defined by Equations (5) and (6):

$$\tau = \mu(\dot{\gamma})\left[\nabla \mathrm{u} + (\nabla \mathrm{u})^{\mathrm{T}}\right] \tag{4}$$

$$\mu(\dot{\gamma}) = \max\left\{\mu_0, \left(\sqrt{\mu_\infty} + \frac{\sqrt{\tau_0}}{\sqrt{\lambda} + \sqrt{\dot{\gamma}}}\right)^2\right\} \tag{5}$$

$$\dot{\gamma} = \sqrt{\nabla \mathrm{u}\left[\nabla \mathrm{u} + (\nabla \mathrm{u})^{\mathrm{T}}\right]} \tag{6}$$

where μ is the dynamic apparent viscosity and $\dot{\gamma}$ is the shear rate. Equation (5) represents the modified Quemada model.[23] The values of the parameters of this model are $\mu_0 = 0.00309$ Pa·s, $\mu_\infty = 0.002654$ Pa·s, $\tau_0 = 0.004360$ Pa, and $\lambda = 0.02181\ \mathrm{s}^{-1}$.

Finally, the particle trajectory was modelled by using the Discrete Phase Model in ANSYS Fluent (ANSYS® Inc.).[24] In a Lagrangian reference frame, this model tracks each particle, which interacts with the continuous phase (i.e., the blood flow) but not with other particles. The governing equation for the particles is the conservation of momentum, expressed as Newton's second law of motion (Equation (7)). Four forces were considered in this study: the virtual mass force (Equation (8)), the pressure gradient force (Equation (9)), the gravitational force (Equation (10)), and the drag force (Equation (11)). Therefore, the conservation of momentum equation per unit particle mass is:

$$\frac{\mathrm{du}^{\mathrm{p}}}{\mathrm{d}t} = \mathrm{f}^{\mathrm{V}} + \mathrm{f}^{\mathrm{P}} + \mathrm{f}^{\mathrm{G}} + \mathrm{f}^{\mathrm{D}} \tag{7}$$

where u^{p} is the particle velocity vector.

$$\mathrm{f}^{\mathrm{V}} = C_V \frac{\rho}{\rho_{\mathrm{p}}}\left(\mathrm{u}^{\mathrm{p}} \nabla \mathrm{u} - \frac{\mathrm{du}^{\mathrm{p}}}{\mathrm{d}t}\right) \tag{8}$$

where C_V is the virtual mass coefficient ($C_V = 0.5$) and ρ_{p} is the density of the particle.

$$\mathrm{f}^{\mathrm{P}} = \frac{\rho}{\rho_{\mathrm{p}}} \mathrm{u}^{\mathrm{p}} \nabla \mathrm{u} \tag{9}$$

$$\mathrm{f}^{\mathrm{G}} = \frac{\rho_{\mathrm{p}} - \rho}{\rho_{\mathrm{p}}} \mathrm{g} \tag{10}$$

where g is the acceleration of gravity, that is, $-9.81\ \mathrm{m/s^2}$ in the direction of the y-axis (see Figure 1).

$$\mathrm{f}^{\mathrm{D}} = \frac{18\mu}{\rho_{\mathrm{p}} d_{\mathrm{p}}^2} \frac{C_D \mathrm{Re}_{\mathrm{p}}}{24} (\mathrm{u} - \mathrm{u}^{\mathrm{p}}) \tag{11}$$

where d_{p} is the particle diameter, C_D is the drag coefficient, and Re_{p} is the particle Reynolds number, shown by Equation (12).

$$\mathrm{Re}_{\mathrm{p}} = \frac{\rho d_{\mathrm{p}} |\mathrm{u}^{\mathrm{p}} - \mathrm{u}|}{\mu} \tag{12}$$

2.4 | Numerical settings

The SIMPLE algorithm was used to solve for the velocity and pressure in a segregated way in the pressure–velocity coupling. Spatial discretization was performed using the least squares cell-based algorithm for gradient computations and the second-order upwind scheme for the convection term of the momentum equations. The second-order algorithm was used for pressure interpolation. A two-way coupled model was used to solve for the continuous phase (blood flow) and the discrete phase (particle transport).

A second-order implicit transient formulation was used in this case with a time step (Δt) of 0.002 s and a cardiac-cycle period (T) of 1 s. The convergence criterion in this study was chosen to attain scaled residuals of 1×10^{-5}.

The governing equations were solved in the commercially available software ANSYS Fluent® 19.2 (ANSYS® Inc.). A 128-core workstation with a clock speed of 2.30 GHz and 128 GB of RAM was used. Each simulation took an average of 15 h to complete.

2.5 | Boundary conditions

The model used to determine the inflow and outflow boundary conditions (BCs) was adapted from a previous work by Aramburu et al.[25,26]; in brief, a literature-based cancer scenario was defined, and the total blood flow and the blood flow split over the outlets were defined according to the tissue volume (distinguishing cancer and healthy tissue) to be perfused and the arterial perfusion value of that tissue. The scenario involves a fictional male patient with metastases of colorectal carcinoma with 30% liver involvement. Table 1 summarises the BCs used for this fictional patient.

The body surface area (BSA) dosimetry method was used to calculate the activity and the number of particles to be administered to the patient. In the case of the fictional male patient from,[6] an activity of 2 GBq must be administered.

Similar numerical models to the one used in this work have been previously validated in in-vitro[27] and in-vivo[28] studies.

2.5.1 | Inlet velocity profile

An inflow BC that accounts for the effect of the upstream tortuosity, which was adapted from previous work,[17] was used. The cited study shows that this type of inflow BC is necessary when using idealised geometries. This realistic inlet profile was derived from a case similar to the one studied in this paper, with a helicity of 37.1 m/s^2.

The magnitude of the velocity was given by Equation (13), and the unit vectors of the velocity at the inlet section of the idealised geometry were taken from.[17] The unit vectors used were defined as axial, radial and tangential components with values of 0.70, 0.45 and 0.55, respectively.

If we assume the catheter to be centred in the inlet section and the flow to be fully developed, the velocity (u) perpendicular to the inlet cross-section can be described by Equation (13):

$$u(r) = \frac{2q}{\pi\left[\left(R_{\text{in}}^4 - R_{\text{out}}^4\right) - \frac{\left(R_{\text{in}}^2 - R_{\text{out}}^2\right)^2}{\ln\left(R_{\text{in}}/R_{\text{out}}\right)}\right]}\left[\left(R_{\text{in}}^2 - R_{\text{out}}^2\right)\frac{\ln\left(r/R_{\text{out}}\right)}{\ln\left(R_{\text{in}}/R_{\text{out}}\right)} - \left(r^2 - R_{\text{out}}^2\right)\right] \tag{13}$$

where q is the inflow (m^3/s), R_{in} (m) is the inner radius of the artery, R_{out} (m) is the outer radius of the catheter, and r is the radial coordinate, with $R_{\text{out}} < r < R_{\text{in}}$. In this particular case, $R_{\text{in}} = 2.5$ mm and $R_{\text{out}} = 0.45$ mm.

TABLE 1 Inflow and outflow boundary conditions (BCs). The blood flow distribution per outlet is represented in percentage values. Velocity inlet and outflow BCs are specific for ANSYS Fluent

Section	Type of boundary conditions	Values	
Inlet	Velocity inlet	Average blood flow = 405.8 mL/min	
Outlet	Outflow	Outlet 01	40.0%
		Outlet 02	40.0%
		Outlet 03	10.0%
		Outlet 04	10.0%
Wall	No-slip condition		

The inlet BC was imposed by using a subroutine that calculated the volumetric blood flow rate and the velocity profile as a function of the arterial radius and the time step. The average flow velocity at the inlet section is shown in Figure 3.

2.5.2 | Microspheres and injection velocity

Commercially available SIR-Spheres® resin microspheres were modelled in this study. The properties of this type of microsphere are shown in Table 2.

A mean particle size of 32 μm and elastic collisions were assumed at the artery and microcatheter walls.

Inside of the microcatheter, the particle-carrying inflow was modelled using the same properties used for blood. A constant particle-carrying fluid flow rate (q_{cath}) was specified in this study. The average velocity can be calculated as the flow rate (18.5 mL/min, taken from a real-life treatment observation by Aramburu et al.[25]) divided by the cross-sectional area of the catheter lumen. Therefore, the particle injection velocity is 0.92 m/s (see Figure 3), and the mass flow rate of particles is 6.8×10^{-5} kg/s.

The particle injection velocity was 0.92 m/s given q_{cath}. According to realistic clinical observations (a series of video recordings of RE treatments were analysed to determine a range of time used by the interventional radiologist to inject the microspheres from the 5-ml syringe), this injection velocity was chosen to be 1.3 times the maximum bloodstream velocity in the cardiac cycle (see Figure 3). "*Velocity inlet*" is the inlet boundary type selected for the particle flow injection, and "*surface*" is the type of injection used in the DPM model for particle release from the internal cross-section at the catheter inlet. This means that an equal mass fraction is injected at each time step ($\Delta t = 0.002$ s) during the 1-s

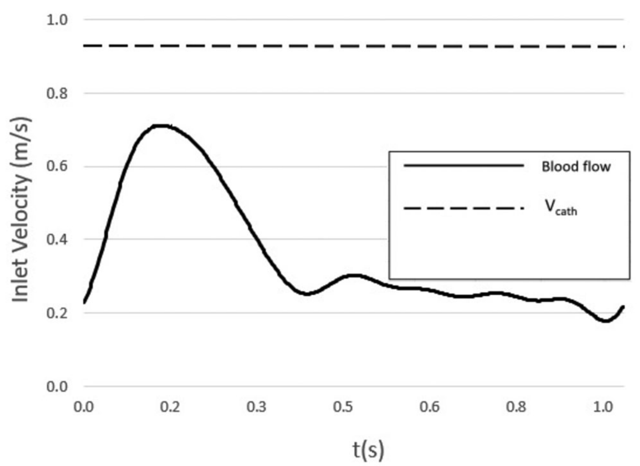

FIGURE 3 Inflow velocity waveform (blood flow) and particle injection velocity (V_{cath})

TABLE 2 Properties of the SIR-Spheres®. In the concentration of particles, we assume the particles are in a 5-ml container

Properties	^{90}Y resin
Manufacturer	Sirtex medical limited
Commercial denomination	SIR-Spheres®
Density (kg/m^3)	1600
Activity (Bq/microsphere)	50
Size Range (μm)	20–60
Mean Size (μm)	32
Injected particles (Activity 2.0 GBq)	40,000,000
Initial concentration (microspheres/ml)	8×10^6

injection (i.e., a cardiac cycle). Particle release occurs in a spatially homogeneous manner through the faces of the inlet of the catheter (the faces that belong to the internal cross section at the catheter inlet).

2.6 | Design concept

The key concept underlying the new catheter design proposed in this paper is the lumen filling phenomenon (lumen filling). It has been reported that for an injection done sufficiently far from a bifurcation and in a tortuous artery, the particle distribution tends to match the flow split because the particles tend to occupy the whole artery lumen before encountering a bifurcation. Lumen filling can be very beneficial in cases where tumours are spread throughout the liver. It is important to stress that tumour arterial perfusion exceeds that of normal tissue. Therefore, if more blood flows towards tumours and the particles travel as the blood does, the particles are more likely to end up in tumours.

Lumen filling could be achieved by modifying two aspects of the catheter design: the direction and the velocity of incorporation of particles in the bloodstream. Particles could cover as much space as possible inside the artery if injected from the lateral surface of the catheter tip in at least four directions perpendicular to each other. Moreover, to obtain a particle trajectory that fills the arterial lumen, the particles must be injected at a high enough velocity that the particles can cross the blood flow streamlines (crossflow effect). For this purpose, the velocity of the particle-carrying fluid must be at least twice the velocity of the blood flow.[29] If particles are to be injected into bloodstream through lateral holes, the size of the holes should be analysed to evaluate the particle-inertial effect.

In this study, different catheters were numerically tested. The common feature of the catheters is the presence of holes in the lateral wall near the tip, hereafter denoted as side-hole catheters. The shapes, positions and numbers of holes were varied. The following section presents the different designs.

2.7 | Design of experiments

Design of Experiments (DoE) is a statistical method for evaluating the effect of several factors on a given response. In this case, an *experiment* is the execution of a numerical simulation.

The main objective of DoE is to determine the factor that has the greatest effect on a relevant response by using the least number of simulations (i.e., computational resources). The response factor chosen is a measure of the flow split and particle distribution matching, which will be fully explained later.

A total of six factors were used to analyse the response factors. The six factors of the side-hole catheters are illustrated in Figure 4.

The *area ratio* parameter was defined as the sum of the outlet areas of the catheter (side-holes plus the catheter lumen cross-sectional area if the tip was open) divided by the inlet area (the catheter lumen cross-sectional area), defined by Equation (14).

$$\mathrm{Area}_{\mathrm{ratio}} = \frac{\sum_{4}^{n} A_{\mathrm{sideholes}} + \mathrm{Tip\ Cross\ Section}_{\mathrm{cath}}}{\mathrm{Cross\ Section}_{\mathrm{cath}}} \tag{14}$$

The area ratio of the six factors ranges from 0.5 to 4.0, with the lower value indicating the tip design with fewer and smaller holes. The base case has an area ratio of 1.

The first row of holes begins 1 mm from the tip of the catheter to avoid particle retention in the catheter tip. A larger distance could result in a radiation-emitting spot near the end of the RE procedure.

2.8 | Simulation planning

Using the statistical software MINITAB® (Minitab, State College, Pennsylvania, USA), 16 runs of simulations were configured, as shown in Table 3. By considering the six design factors, a fractional design with the qualities of 4 was chosen. This type of design tests only a subset of all possible factor combinations of factors, which is sufficient to examine all the main effects and two-way interactions while requiring fewer simulations than a full factorial design.

Fractional Design

Main Factors	Low	High
Side-hole diameter (mm)	0.23	0.40
Number of rows	1	2
Angle between holes	0°	120°
Side-hole shape	Circular	Elliptical
Distance between rows (mm)	1	3
Front opening	Closed	Open

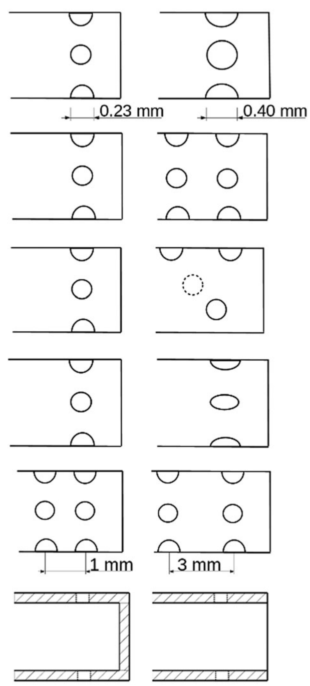

FIGURE 4 Factor settings for side-hole catheters

The runs shown in Table 3 were all executed at two distances from the bifurcation: 30 and 10 mm. Additionally, a reference case, labelled *case 0*, was carried out with a standard end-hole microcatheter.

Each simulation consists of five 1-s cardiac cycles. The first cycle (t = −1 s to t = 0 s) is intended to eliminate the influence of the initial value of the simulation. During the second cycle (t = 0 s to t = 1 s), the microspheres are injected into the computational domain. Three additional cycles are simulated to ensure that most of the particles exit the computational domain (t = 1 s to t = 4 s).

2.9 | Post-processing

Two types of post-processing analyses were used in this study. First, the percentage of particles exiting each outlet was considered. This parameter is essential in assessing the alignment of the particle distribution and the flow split. This percentage was calculated by dividing the mass of particles exiting each outlet by the total particle mass injected.

In addition to the percentage of particle distribution, the *matching deviation index* (MDI) was defined to relate the particle distribution and flow rate in each outlet. The MDI is the average number of liver segments for the difference, in each segment, between the particle distribution percentage and the blood flow split percentage. The MDI is presented in Equation (15):

$$\mathrm{MDI} = \frac{1}{N}\sum_{s=1}^{N}\left|\frac{N_{\mathrm{p},s}}{\sum_{s=1}^{N} N_{\mathrm{p},s}} - \frac{q_s}{\sum_{s=1}^{4} q_s}\right| \cdot 100\,(\text{percent points}) \tag{15}$$

where s is the outlet counter from 1 to N (in this case, $N = 4$) and $N_{\mathrm{p},s}$ is the total amount of targeted particles in outlet s with a blood flow of q_s. In this specific case, the MDI is bounded between 0 (perfectly matching) and 45 percentage points (when all of the particles exit only by the lower flow rate outlet).

TABLE 3 Summary of runs (simulations) of fractional design

Run number	Diameter (mm)	Number of rows	Angle between holes	Hole shape	Distance between rows (mm)	Front	Area ratio
I	0.23	1	0°	Circular	1	Opened	1.5
II	0.23	1	0°	Ellipse	1	Closed	0.5
III	0.40	1	0°	Circular	3	Closed	1.5
IV	0.40	1	0°	Ellipse	3	Opened	2.5
V	0.23	2	0°	Circular	3	Closed	1.0
VI	0.23	2	0°	Ellipse	3	Opened	2.0
VII	0.40	2	0°	Circular	1	Opened	4.0
VIII	0.40	2	0°	Ellipse	1	Closed	3.0
IX	0.23	1	120°	Circular	3	Opened	1.5
X	0.23	1	120°	Ellipse	3	Closed	0.5
XI	0.40	1	120°	Circular	1	Closed	1.5
XII	0.40	1	120°	Ellipse	1	Opened	2.5
XIII	0.23	2	120°	Circular	1	Closed	1.0
XIV	0.23	2	120°	Ellipse	1	Opened	2.0
XV	0.40	2	120°	Circular	3	Opened	4.0
XVI	0.40	2	120°	Ellipse	3	Closed	3.0

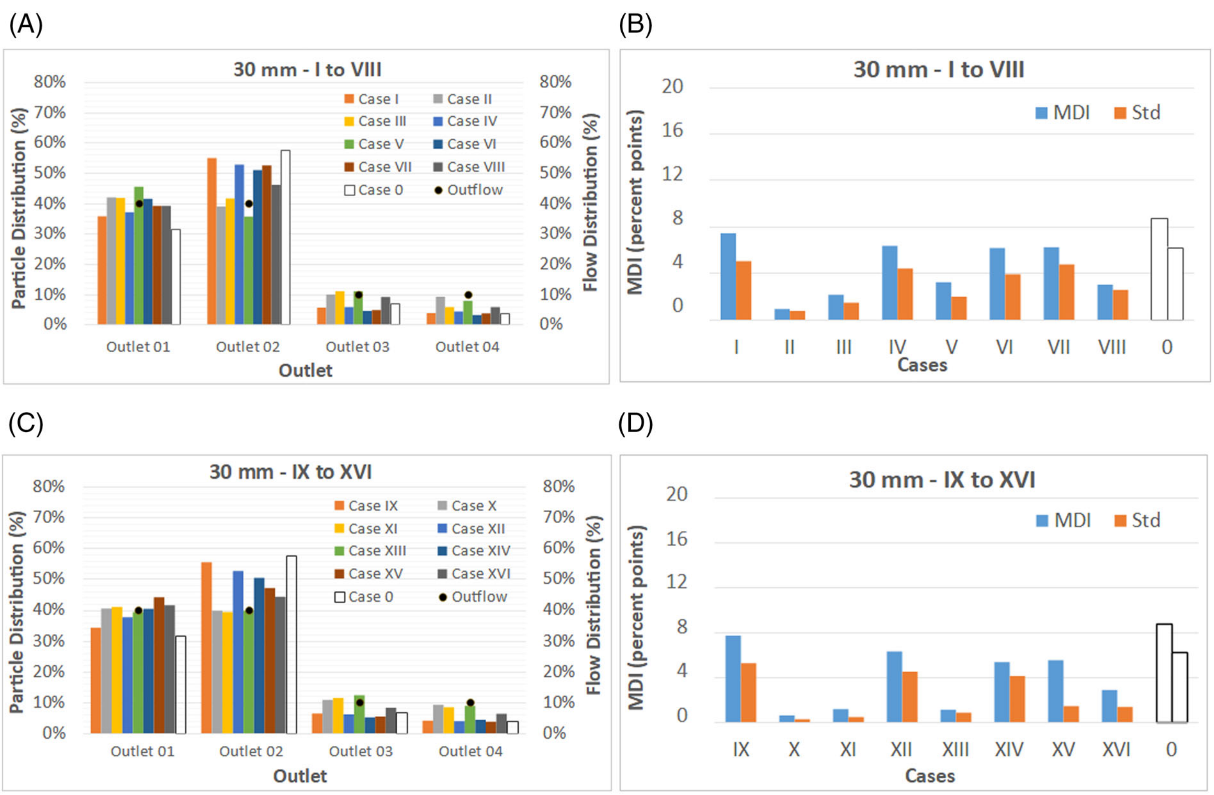

FIGURE 5 Particle distribution and blood flow distribution in the outlets and matching deviation index (MDI) values per case with an injection point at 30 mm from the bifurcation. (A) Outlet-to-outlet particle distribution for simulations I to VIII, including *case 0*. (B) MDI and standard deviation for simulations I to VIII. (C) Outlet-to-outlet particle distribution for simulations IX to XVI, including *case 0*. (D) MDI and standard deviation for simulations IX to XVI

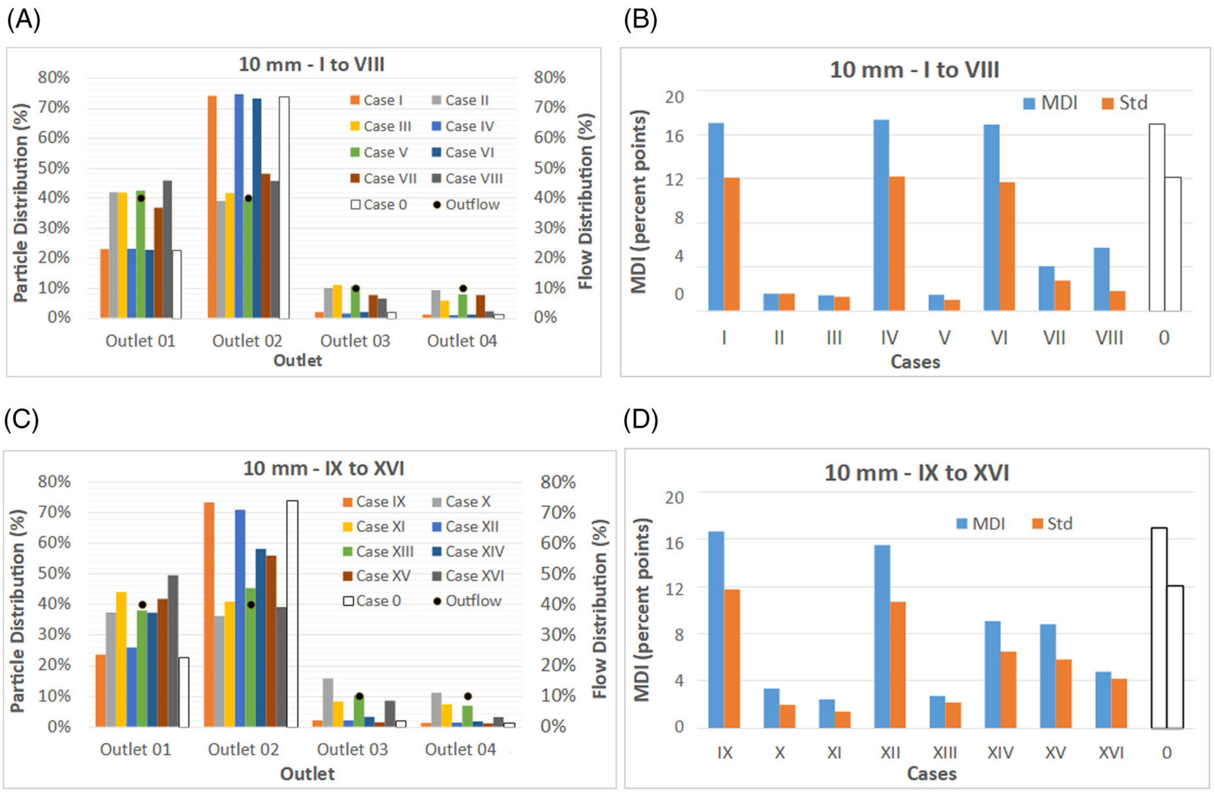

FIGURE 6 Particle distribution and blood flow distribution in the outlets and matching deviation index (MDI) values per case with an injection point at 10 mm from the bifurcation. (A) Outlet-to-outlet particle distribution for simulations I to VIII, including *case 0*. (B) MDI and standard deviation for simulations I to VIII. (C) Outlet-to-outlet particle distribution for simulations IX to XVI, including *case 0*. (D) MDI and standard deviation for simulations IX to XVI

The second post-processing analysis is related to the mixing of particles in the artery lumen and the statement by Aramburu et al.[10] about the importance of injecting sufficiently far from a bifurcation to obtain a particle distribution that matches the blood flow distribution. The parameter was the particle distribution in cross-sections in a time-integrated way, as this is a measure of the degree of matching between the flow distribution and the particle distribution.

To further analyse the particle dispersion on a surface of interest, an index is defined to evaluate the degree to which the particles are spread out in the artery lumen in the simulations, denoted as the coefficient of variation, CoV, as explained in.[17] This index represents the ratio between the standard deviation, σ, and the average, $\overline{X}$, of the particles located in the cells at a specific cross-section of the artery and is defined by Equation (16):

$$\mathrm{CoV} = \frac{\sigma}{\overline{X}} \tag{16}$$

The particle concentration in a group of cells in a specific cross-section of the artery is determined by the unsteady statistics variable *accumulative particles in cell*, ϕ, defined in ANSYS® Fluent 19.2.[24]

When the CoV is 0, the variable is fully homogeneous, implying that the particles are evenly dispersed throughout the arterial cross-section. A high CoV value indicates that the particles are concentrated in a particular zone of the arterial cross-section.

3 | RESULTS AND DISCUSSION

The goal of this section is to analyse the importance and influence of catheter design factors on downstream particle distribution while taking into account the lumen filling phenomenon in the PHA, where the particles are delivered into the arterial vasculature.

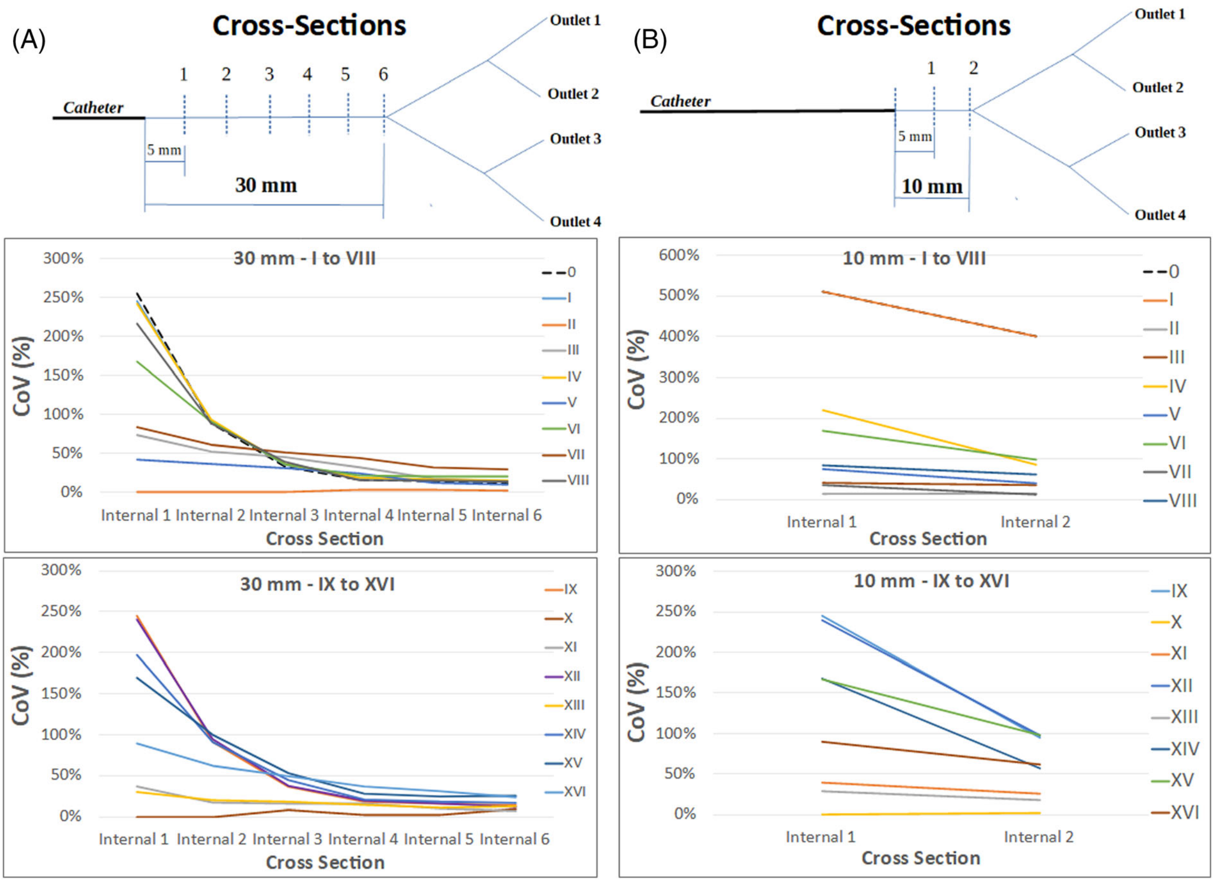

FIGURE 7 CoV along level I for the simulations with (A) the injection point 30 mm from the bifurcation and (B) the injection point 10 mm from the bifurcation

Figures 5 and 6 show the results in terms of both outlet-to-outlet particle distribution and the MDI for injections 30 and 10 mm from the PHA bifurcation, respectively. In these figures, outlets are shown on the *x*-axis, the percentage of particles that exit through each outlet are shown on the primary *y*-axis, and the blood flow distribution per outlet is shown on the secondary *y*-axis. In Figures 5B and 6B, the cases are shown on the *x*-axis and the MDI and the standard deviation (referred to as the dispersion from the average values of particle distribution in each outlet for a specific case) are shown on the *y*-axis.

The reference case, denoted as case 0, has the worst results in terms of particle distribution, as indicated by the highest value of the MDI (see Figures 5B,D and 6B,D). In this catheter, because there are no side holes, the particles are released in one longitudinal direction. Therefore, only the spiral flow in the artery promotes lumen filling.

In Figure 5B, the lower MDI values (below 5 percentage points) correspond to side-hole catheters with the frontal section closed. Despite the presence of side holes in the other designs, the presence of an open frontal section causes the particles to follow the least resistant and simplest path through the frontal section.The results are similar when the injection is done 10 mm from the bifurcation. The MDI values for designs with open frontal section are higher than the same cases for injections at 30 mm, most of them exceeding 12 percentage points. In these cases, the injected particle lumen filling is not promoted due to the proximity of a bifurcation, especially when the particles are injected in the artery with the standard end-hole microcatheter (case 0). When particles are released from the side holes, lumen filling is promoted near the catheter tip, improving the MDI value.

Regarding the relative position of the catheter tip with respect to a downstream bifurcation, closed frontal section catheter designs produce the best results in terms of MDI values. For this design, the particle distributions are independent of the tip distance to the bifurcation. For open frontal section catheter designs, the results do depend on the tip distance to the bifurcation. However, when compared to the same simulations with a distance of 10 mm between the tip and the bifurcation, when the distance between the tip and the downstream bifurcation is 30 mm, the particle trip appears to be long enough to promote lumen filling and improve the MDI.

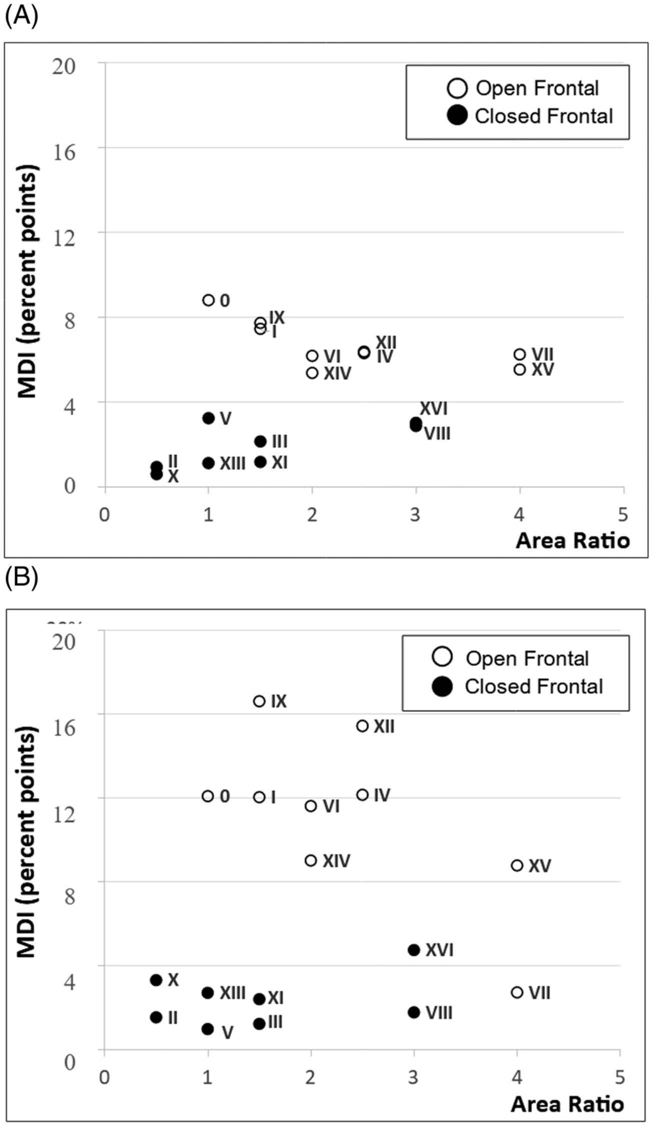

FIGURE 8 Matching deviation index (MDI) at several area ratio parameters for the simulations (A) with an injection point at 30 mm from the bifurcation and (B) with an injection point at 10 mm from the bifurcation

Figure 7 shows the value of CoV at different cross-sections along the PHA. In the cases with the injection 30 mm from the bifurcation (see Figure 7A), all the cases including case 0 result in CoV values below 50%. For the injection near the bifurcation, only the side-hole catheters with a closed frontal section and an area ratio below 3.0 (cases II, III, V, X, XI, and XIII) result in CoV values below 50%. Therefore, the side-hole catheter design is of utmost importance for promoting lumen filling when a bifurcation is close to the injection point.

In addition, the trend of the reported MDI and CoV values suggests the existence of the following relationship: the lower the CoV, the lower is the MDI, and vice versa. This relationship is due to the lumen filling effect, caused primarily by the side-hole catheter design and, to a lesser extent, by the helical blood flow.Figure 8 shows the relationship between the MDI and the area ratio for the cases simulated with the catheter tip 30 mm from the bifurcation (Figure 8A) and for the cases simulated with the catheter tip 10 mm from the bifurcation (Figure 8B). The results show that side-hole designs with a closed frontal section perform better (lower MDI values).

Regarding the area ratio, lower area ratios (i.e., lower side-hole surface area) result in a greater crossflow effect, which is not always beneficial in terms of MDI, especially if the frontal section is open. When the frontal section is closed, the high velocity at which the particles are delivered from the side holes promotes lumen filling and improves the MDI values.

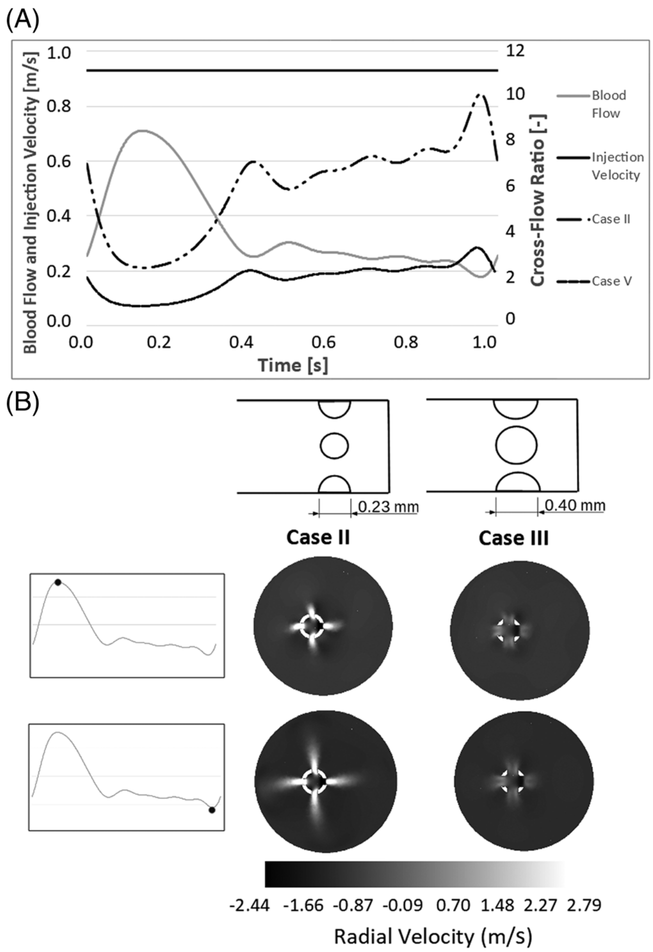

FIGURE 9 (A) Ratio of the velocity to the injection velocity in one cardiac cycle for cases 0, II, and III (when injecting 30 mm from the bifurcation). (B) Contour plots of the radial velocity for side-hole design cases (II and III) at the injection surface

The results suggest that there is an optimum range for catheter design factors to produce a better response. Considering the injection velocity used in this study, a side-hole catheter with an area ratio below 2.0 and a closed frontal section generates an MDI below 4 percentage points. However, even if lateral holes are present, if the frontal section end is open, few particles are infused from the side holes because most of the particles follow a straight minimum-resistance trajectory. When this occurs, the MDI is greater than 5 percentage points.The key concept in this study is the crossflow effect. This effect is defined as the phenomenon in which the released particle-carrying fluid and the particles are able to cross the blood flow streamlines and to follow a perpendicular path line. For this purpose, the fluid in which micron-sized particles are diluted must be delivered with sufficient velocity from the lateral holes of the side-hole catheter. In other words, the relative velocity (defined as the difference between the particle and blood flow velocity) must be sufficiently high. This effect is very difficult to promote when the frontal section is open because the particle-carrying flow tends to flow towards the least-resistance straight path. However, if the frontal section is closed, the crossflow effect is promoted, which enhances the lumen filling effect. When the frontal section is closed, a greater crossflow effect will be promoted as the area ratio decreases (because of the mass conservation principle). Figure 7 shows that the lower the area ratio (e.g., simulations II, V, X and XIII), the lower is the CoV along the PHA.

To assess the crossflow effect, Figure 9 compares three relative velocity profiles for cases 0, II and III when the injection is done 30 mm from the bifurcation and shows the velocity contours at the injection plane for two temporal points in the cardiac cycle. Regarding the velocity profiles, Figure 9A shows, for a time interval of one cardiac cycle, the blood flow velocity and the injection velocity (considering the proximal end of the catheter, not the distal end where the particles are delivered into the bloodstream) on the primary *y*-axis, and the velocity ratio on the secondary *y*-axis. The velocity ratio is the ratio of the area-weighted average particle velocity in the catheter side holes to the area-weighted average blood flow velocity in the artery lumen. The velocity ratio follows the same pattern over time: it peaks when the blood flow velocity is at its lowest. The greatest crossflow effect takes place at that temporal point (i.e., the end of diastole). For side-hole catheter designs with a closed frontal section, the time-averaged velocity ratio is related to the area ratio parameter: the greater the area ratio, the lower is the velocity ratio because the greater the hole surface area, the lower is the particle-carrying fluid velocity (mass conservation principle). For case 0, the area ratio and the average velocity ratio are 1.0 and 3.06, respectively; for case II: 0.50 and 5.98; and for case III: 1.5 and 2.01. Therefore, one might think that "the smaller the area ratio is, the greater the velocity ratio, the greater the crossflow effect, the better the MDI, and the better the performance of the side-hole catheter design". However, the results suggest that there is a minimum level of crossflow beyond which a lower side-hole area (or area ratio) plays only a minor role in obtaining an even better MDI. In other words, above a certain area ratio, the performance improvement of the new catheter will be small.

Figure 9B shows the radial velocity at the injected times for cases II and III at the systolic peak (maximum blood flow velocity, minimum crossflow effect) and at the end diastole (minimum blood flow velocity, maximum crossflow effect) temporal points when the injection was done 30 mm away from the bifurcation. These contours provide a visual representation of the crossflow effect, which is greater when the area ratio is smaller (case II) and when the blood flow velocity is smaller (end diastole). It is also important to consider that diastole, where the greatest crossflow effect is promoted, lasts for 60% of the cardiac cycle, which is beneficial in terms of generating a crossflow effect that promotes the lumen filling effect.

4 | CLINICAL IMPLICATIONS

In this study, we present a new side-hole catheter design that improves the treatment outcome in terms of flow splitting and particle outlet-to-outlet distribution matching when compared to the performance of a standard end-hole microcatheter.

Downstream particle distribution can be affected by factors that the interventional radiologist cannot reliably control, such as the cross-sectional or longitudinal catheter tip position in the artery. From the medical procedure point of view, an interesting advantage of the presented catheter is the promotion of conditions that make the particle distribution similar to the flow split, regardless of the catheter position. In addition to the catheter tip location, there are multiple parameters that could affect particle transport in RE treatment (e.g., hepatic arterial morphology, tumour type, size, and location, and injection velocity).

This side-hole catheter is an excellent choice for patients who have tumours in all segments downstream of the catheter tip. Currently, this occurs in most cases. This catheter would not create any further advantages if the previous statement was not true, or if there was a single tumour and a superselective treatment that directly reached the tumour could be performed.

In summary, we are not presenting a universal catheter design, but rather one that has the potential to improve the performance of conventional catheters in many patients, which is important when planning a patient-specific RE procedure.

5 | CONCLUSIONS

In this study, a side-hole catheter was designed and assessed using an idealised hepatic artery and physiologically realistic BCs. The desired effect was to promote lumen filling near the catheter tip, thereby improving the alignment between the particle distribution and the blood flow split. The use of the presented side-hole catheter could improve RE outcomes in patients with tumours distributed in segments downstream from the catheter tip.

A side-hole catheter with side holes located on the outer wall near the catheter tip and a closed frontal tip produced the best results. In this case, the crossflow effect explains the physical behaviour of the particle trajectory, which is related to the direction and the relative velocity with which the particles are injected into the artery lumen from the lateral sides of the catheter. The particle dispersion will be greater if the crossflow is sufficiently high.

The smaller the area ratio is, the greater the velocity ratio, the greater the crossflow effect, the better the MDI, and the better the performance of the side-hole catheter design. However, the results suggest that there is a minimum level of crossflow beyond which a lower side-hole area (or area ratio) plays a minor role in obtaining a better MDI.

Case II (side-hole catheter) produced the best MDI results with 0.9 percentage points when the injection point was 30 mm from the bifurcation and 1.5 percentage points when the injection point was 10 mm from the bifurcation. In case 0 (end-hole catheter), the MDIs were 23.8 and 17.0 percentage points for the 30 and 10 mm cases, respectively.

Future studies must assess the performance of the new catheter design in patient-specific cases, such as cancer type and sizes, increased injection velocities and spatial catheter tip positions.

ACKNOWLEDGEMENTS

This research was funded by the Spanish Government through project DPI 2015-68985-R. The authors gratefully acknowledge the support of Cátedra Fundación Antonio Aranzábal-Universidad de Navarra and the financial support of the first author via an ANID Scholarship (*Becas Chile*) and Proyecto VRIEA-PUCV 039.356/2021.

DATA AVAILABILITY STATEMENT

The data that support the findings of this study are available from the corresponding author upon reasonable request.

ORCID

Julio Ortega https://orcid.org/0000-0001-5472-8791
Raúl Antón https://orcid.org/0000-0003-1329-5891
Juan Carlos Ramos https://orcid.org/0000-0002-2560-1051
Alejandro Rivas https://orcid.org/0000-0001-7755-8748
Gorka S. Larraona https://orcid.org/0000-0001-9055-4995
Bruno Sangro https://orcid.org/0000-0002-4177-6417
José Ignacio Bilbao https://orcid.org/0000-0002-8265-9276
Jorge Aramburu https://orcid.org/0000-0002-2911-3397

REFERENCES

1. Bray F, Ferlay J, Soerjomataram I, Siegel RL, Torre LA, Jemal A. Global cancer statistics 2018: GLOBOCAN estimates of incidence and mortality worldwide for 36 cancers in 185 countries. *CA Cancer J Clin*. 2018;68(6):394-424. doi:10.3322/caac.21492
2. Sangro B, Salem R. Transarterial chemoembolization and radioembolization. *Semin Liver Dis*. 2014;34(4):435-443. doi:10.1055/s-0034-1394142
3. Ma J, Gimenez JM, Sandow T, et al. Intraarterial liver-directed therapies: the role of interventional oncology. *Ochsner J*. 2017;17(4):412-416. doi:10.1043/TOJ-17-0037
4. Murthy R, Kamat P, Nuñez R, Salem R. Radioembolization of yttrium-90 microspheres for hepatic malignancy. *Semin Interv Radiol*. 2008;25(1):48-57. doi:10.1055/s-2008-1052306
5. Sangro B, Bilbao JI, Boan J, et al. Radioembolization using 90Y-resin microspheres for patients with advanced hepatocellular carcinoma. *Int J Radiat Oncol Biol Phys*. 2006;66(3):792-800. doi:10.1016/j.ijrobp.2006.05.065
6. Memon K, Lewandowski RJ, Kulik L, Riaz A, Mulcahy MF, Salem R. Radioembolization for primary and metastatic liver cancer. *YSRAO*. 2011;21(4):294-302. doi:10.1016/j.semradonc.2011.05.004
7. Kleinstreuer C, Feng Y, Childress E. Drug-targeting methodologies with applications: a review. *World J Clin Cases*. 2014;2(12):742-756. doi:10.12998/wjcc.v2.i12.742
8. Aramburu J, Antón R, Rivas A, Ramos JC, Sangro B, Bilbao JI. Liver Radioembolization: an analysis of parameters that influence the catheter-based particle-delivery via CFD. *Curr Med Chem*. 2020;27(10):1600-1615. doi:10.2174/0929867325666180622145647
9. Childress EM, Kleinstreuer C. Computationally efficient particle release map determination for direct tumor-targeting in a representative hepatic artery system. *J Biomech Eng*. 2013;136(1):011012. doi:10.1115/1.4025881
10. Aramburu J, Antón R, Rivas A, Ramos JC, Sangro B, Bilbao JI. The role of angled-tip microcatheter and microsphere injection velocity in liver radioembolization: a computational particle-hemodynamics study. *International Journal for Numerical Methods in Biomedical Engineering*. 2017;33(12):e2895. doi:10.1002/cnm.2895
11. Aramburu J, Antón R, Rivas A, Ramos JC, Sangro B, Bilbao JI. Numerical investigation of liver radioembolization via computational particle–hemodynamics: the role of the microcatheter distal direction and microsphere injection point and velocity. *J Biomech*. 2016; 49(15):3714-3721. doi:10.1016/j.jbiomech.2016.09.034
12. Basciano CA, Kleinstreuer C, Kennedy AS, Dezarn WA, Childress E. Computer modeling of controlled microsphere release and targeting in a representative hepatic artery system. *Ann Biomed Eng*. 2010;38(5):1862-1879. doi:10.1007/s10439-010-9955-z
13. Xu Z, Jernigan S, Kleinstreuer C, Buckner GD. Solid tumor embolotherapy in hepatic arteries with an anti-reflux catheter system. *Ann Biomed Eng*. 2016;44(4):1036-1046. doi:10.1007/s10439-015-1411-7
14. Aramburu J, Antón R, Rivas A, Ramos JC, Sangro B, Bilbao JI. Computational assessment of the effects of the catheter type on particle–hemodynamics during liver radioembolization. *J Biomech*. 2016;49(15):3705-3713. doi:10.1016/j.jbiomech.2016.09.035

15. van den Hoven AF, Lam MGEH, Jernigan S, van den Bosch MAAJ, Buckner GD. Innovation in catheter design for intra-arterial liver cancer treatments results in favorable particle-fluid dynamics. *J Exp Clin Cancer Res*. 2015;34(1):74. doi:10.1186/s13046-015-0188-8
16. Guyennon A. Perfusion characterization of liver metastases from endocrine tumors: computed tomography perfusion. *World J Radiol*. 2010;2(11):449-454. doi:10.4329/wjr.v2.i11.449
17. Ortega J, Antón R, Ramos JC, et al. On the importance of spiral-flow inflow boundary conditions when using idealized artery geometries in the analysis of liver radioembolization: a parametric study. *International Journal for Numerical Methods in Biomedical Engineering*. 2020;36(6):1-21. doi:10.1002/cnm.3337
18. Hiatt JR, Gabbay J, Busuttil RW. Surgical anatomy of the hepatic arteries in 1000 cases. *Ann Surg*. 1994;220(1):50-52. doi:10.1097/00000658-199407000-00008
19. Zamir M. On fractal properties of arterial trees. *J Theor Biol*. 1999;197(4):517-526. doi:10.1006/jtbi.1998.0892
20. Zamir M, Chee H. Branching characteristics of human coronary arteries. *Can J Physiol Pharmacol*. 1986;64(6):661-668. doi:10.1139/y86-109
21. Schreiner W, Neumann M, Neumann F, et al. The branching angles in computer-generated optimized models of arterial trees. *J Gen Physiol*. 1994;103(6):975-989. doi:10.1085/jgp.103.6.975
22. Carlisle KM, Halliwell M, Read AE, Wells PN. Estimation of total hepatic blood flow by duplex ultrasound. *Gut*. 1992;33(1):92-97. doi:10.1136/gut.33.1.92
23. Buchanan JR, Kleinstreuer C, Comer JK. Rheological effects on pulsatile hemodynamics in a stenosed tube. *Comput Fluids*. 2000;29(6):695-724. doi:10.1016/S0045-7930(99)00019-5
24. ANSYS Inc. ANSYS Fluent Tutorial Guide 18. 2018;15317(April):724-746. doi:10.1016/0140-3664(87)90311-2
25. Aramburu J, Antón R, Rivas A, Ramos JC, Sangro B, Bilbao JI. Computational particle–haemodynamics analysis of liver radioembolization pretreatment as an actual treatment surrogate. *International Journal for Numerical Methods in Biomedical Engineering*. 2017;33(2):e02791. doi:10.1002/cnm.2791
26. Aramburu J, Antón R, Rivas A, Ramos JC, Sangro B, Bilbao JI. Liver cancer arterial perfusion modelling and CFD boundary conditions methodology: a case study of the haemodynamics of a patient-specific hepatic artery in literature-based healthy and tumour-bearing liver scenarios. *International Journal for Numerical Methods in Biomedical Engineering*. 2016;32(11):e02764. doi:10.1002/cnm.2764
27. Richards AL, Kleinstreuer C, Kennedy AS, Childress E, Buckner GD. Experimental microsphere targeting in a representative hepatic artery system. *IEEE Trans Biomed Eng*. 2012;59(1):198-204. doi:10.1109/TBME.2011.2170195
28. Antón R, Antoñana J, Aramburu J, et al. A proof-of-concept study of the in-vivo validation of a computational fluid dynamics model of personalized radioembolization. *Sci Rep*. 2021;11(1):Dec. doi:10.1038/s41598-021-83414-7
29. Basciano CA, Kleinstreuer C, Kennedy AS. Computational fluid dynamics modeling of 90Y microspheres in human hepatic tumors. *J Nucl Med Radiat Ther*. 2011;2:112. doi:10.4172/2155-9619.1000112

How to cite this article: Ortega J, Antón R, Ramos JC, et al. Computational study of a novel catheter for liver radioembolization. *Int J Numer Meth Biomed Engng*. 2022;38(4):e3577. doi:10.1002/cnm.3577